Deterministic Magnetization Switching by Voltage Control of Magnetic Anisotropy and Dzyaloshinskii-Moriya Interaction under an In-Plane Magnetic Field

Hiroshi Imamura,[1,*] Takayuki Nozaki,[1] Shinji Yuasa,[1] and Yoshishige Suzuki[1,2]

[1] *National Institute of Advanced Industrial Science and Technology (AIST), Spintronics Research Center, Tsukuba, Ibaraki 305-8568, Japan*

[2] *Graduate School of Engineering Science, Osaka University, Toyonaka, Osaka 560-8531, Japan*

(Received 7 December 2017; revised manuscript received 21 June 2018; published 16 November 2018)

Based on micromagnetic simulations, magnetization switching in a triangle magnetic element by voltage control of the magnetic anisotropy and Dzyaloshinskii-Moriya interaction under an in-plane magnetic field is proposed. The proposed switching scheme is not toggle switching but deterministic switching, in which the magnetic state is determined by the polarity of the applied voltage pulse. The mechanism and conditions for the switching are clarified. The results provide a fast and low-power writing method for magnetoresistive random-access memories.

DOI: 10.1103/PhysRevApplied.10.054039

I. INTRODUCTION

Voltage control of magnetic anisotropy (MA) in a thin ferromagnetic film has attracted much attention as a key phenomenon for low-power spin manipulation [1–13]. The first experimental demonstration was reported by Weisheit *et al.* [1]. They showed that the MA of ordered iron-platinum (FePt) and iron-palladium (FePd) intermetallic compounds can be reversibly modified by an applied electric field when immersed in an electrolyte. Two years later, Maruyama *et al.* observed a voltage-induced change of magnetic anisotropy in an all-solid-state device with a MgO dielectric layer [2], including MgO-based magnetic tunnel junctions [3], which paved the way for the voltage-controlled magnetic random-access memory (VCMRAM) with low-power consumption [4–13].

The writing procedure of a VCMRAM is as follows. The memory cell consists of a perpendicularly magnetized recording layer and is subjected to an in-plane external magnetic field. The voltage pulse is applied to the cell to remove the MA and induce the precession of the magnetic moments around the external magnetic field. If the voltage is turned off at one-half period of precession, the magnetization switching completes. Since this is the toggle mode switching a preread is neccessary, i.e., one has to read the information stored in the cell before writing. It is highly desired to develop another fast and low-power writing method to avoid the cost of preread.

Recently, a growing interest in the interface Dzyaloshinskii-Moriya interaction (DMI) [14–28] emerged because of its relevance to noncollinear magnetic structures such as magnetic walls and magnetic skyrmions [29]. The value of the DMI constant ranges from 0.05 to 1 mJ/m^2 depending on the materials. In 2015, Nawaoka *et al.* found that the interface DMI in the Au/Fe/MgO artificial multilayer can be controlled by voltage [27]. Although the voltage-induced change in the DMI constant is estimated to be as small as 40 nJ/m^2 at 1 V, the observation showed the possibility of manipulating magnetization by using voltage-induced changes of MA and DMI.

In this paper, we perform micromagnetic simulations and show that voltage-induced changes of magnetic anisotropy and interface DMI can switch the magnetization of a perpendicularly magnetized right triangle under an in-plane magnetic field. The magnetic state after the voltage pulse is determined by the polarity of the voltage irrespective of the initial magnetic state.

II. BASIC CONCEPT OF SWITCHING

We consider magnetization switching in a perpendicularly magnetized right-triangle nanomagnet shown in Fig. 1(a) by application of a voltage pulse shown in Fig. 1(b). There are two magnetic states at equilibrium: one is an up-polarized state and the other is a down-polarized state. Both the MA constant (K) and the DMI constant (D) are assumed to be voltage controllable. Voltage dependence of K has been studied by several groups [3,6,7,30]. Some have reported linear voltage dependence [3,7] and others have reported nonlinear voltage dependence [6,30]. In this study, K is assumed to be a symmetric function of the voltage (V) and decreases with an increase or decrease

*h-imamura@aist.go.jp

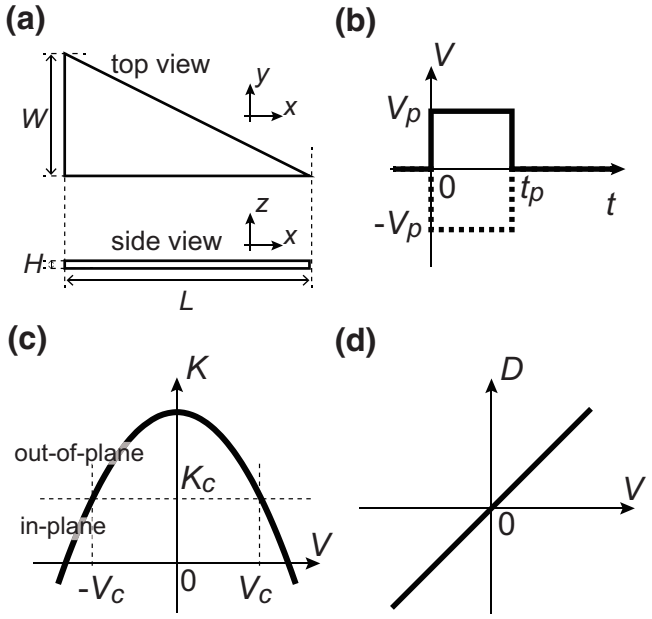

FIG. 1. (a) Top and side views of a right-triangle element, where the width, length, and height are presented by W, L, and H, respectively. (b) Time (t) dependence of the voltage (V) for the positive (solid) and negative (dotted) voltage pulse with an amplitude of V_p, where t_p denotes the duration of the pulse. (c) V dependence of the effective anisotropy constant (K), where K_c denotes the critical value below which the magnetization becomes the almost in-plane polarized state. $\pm V_c$ denotes the corresponding critical voltages. (d) V dependence of the DMI constant (D).

of V as shown in Fig. 1(c). There is a critical value, K_c, below which most magnetic moments are aligned in the plane. Since K is assumed be a symmetric function of V, the almost in-plane magnetic state is realized by application of the voltage of $|V| \geq V_c$, where V_c is the critical voltage.

Itshould be noted that the demagnetization field at the corners is much weaker than that in the middle. Even at $|V| = V_c$, the magnetic moments at the corners have a considerable out-of-plane component. One can modify the direction of the magnetic moments at the corners via the voltage control of D. The DMI is the noncollinear exchange interaction and rotates the magnetic moments. The magnitude of D represents the period of rotation. The sign of D represents the direction of rotation, i.e., clockwise or anticlockwise. D is assumed to be an antisymmetric function of V as shown in Fig. 1(d). The direction of rotation of magnetic moments and, therefore, the direction of magnetic moments at the corners can be controlled by the sign of V. Although a material having both the symmetric V-dependent K and antisymmetric V-dependent D has not been fabricated yet, it is important to study the mechanism and conditions for deterministic switching based on micromagnetic simulations prior to the experiments.

After the voltage is turned off, the magnetic moments relax to the up-polarized or down-polarized state depending on the magnetic configuration at the corners. In the relaxation process, the corners act as nucleation sites. The switching mode is not the coherent rotation but the domain wall displacement. To push the domain wall out of the magnetic element smoothly, the magnetic element should have a low symmetry shape like a right triangle, as shown in Fig. 1(a).

III. SIMULATION MODEL

The micromagnetic simulations are performed by using the software package MuMax3 [31]. We solve the Landau-Lifshitz equation defined as

$$\frac{\partial \boldsymbol{m}}{\partial t} = -\frac{\gamma}{1+\alpha^2}\left\{\boldsymbol{m} \times B_{\text{eff}} + \alpha\left[\boldsymbol{m} \times (\boldsymbol{m} \times B_{\text{eff}})\right]\right\}, \quad (1)$$

where $\boldsymbol{m}$ is the magnetization unit vector, t is time, γ is the gyromagnetic ratio, and α is the Gilbert damping constant. The effective field

$$\boldsymbol{B}_{\text{eff}} = \boldsymbol{B}_{\text{ext}} + \boldsymbol{B}_{\text{demag}} + \boldsymbol{B}_{\text{exch}} + \boldsymbol{B}_{\text{anis}}, \quad (2)$$

comprises the external field $\boldsymbol{B}_{\text{ext}}$, the demagnetizing field $\boldsymbol{B}_{\text{demag}}$, the exchange field $\boldsymbol{B}_{\text{exch}}$, and the anisotropy field $\boldsymbol{B}_{\text{anis}}$. The external field is applied in the positive x direction: $\boldsymbol{B}_{\text{ext}} = B_{\text{ext}}\boldsymbol{e}_x$, where $\boldsymbol{e}_i$ $(i = x, y, z)$ represents the unit vector in the direction of the positive i axis. The definition of the Cartesian coordinates is given in Fig. 1(a). The anisotropy field is given by

$$\boldsymbol{B}_{\text{anis}} = \frac{2K}{M_s H} m_z \boldsymbol{e}_z, \quad (3)$$

where M_s is the saturation magnetization and H is the height of the triangle element, as shown in Fig. 1(a). The exchange field comprises the Heisenberg exchange interaction term and the DMI term as

$$\boldsymbol{B}_{\text{exch}} = \frac{2A}{M_s}\nabla^2 \boldsymbol{m} + \frac{2D}{M_s}\left(\frac{\partial m_z}{\partial x}, \frac{\partial m_z}{\partial y}, -\frac{\partial m_x}{\partial x} - \frac{\partial m_y}{\partial y}\right), \quad (4)$$

where A is the exchange stiffness constant for the Heisenberg interaction.

The width, length, and height of the triangle element are assumed to be $W = 32$ nm, $L = 64$ nm, and $H = 2$ nm, respectively. The system is divided into cubic cells of side length 2 nm. The following material parameters are assumed: saturation magnetization $M_s = 1.35$ MA/m and exchange stiffness constant $A = 10$ pJ/m. The Gilbert damping constant α ranges from 0.1 to 1. The MA constant during the pulse (K_p) ranges from 0 to 2 mJ/m^2. The MA constant at $V = 0$ is assumed to be 4 mJ/m^2. The DMI constant during the pulse (D_p) ranges from 0.01 to 2 mJ/m.

The DMI constant at $V = 0$ is assumed to be 0. The shape of the voltage pulse is shown in Fig. 1(b), where V_p and t_p are the amplitude and the duration of the pulse.

IV. RESULTS AND DISCUSSIONS

Figures 2(a)–2(d) show the typical examples of the magnetization dynamics. The value of α is assumed to be 1 to suppress the precessional motion during the pulse. The x, y, and z components of the space-averaged magnetization unit vector are plotted by the blue dotted, red dashed, and black solid curves, respectively. The external magnetic field of $B_{\rm ext} = 10$ mT is applied in the positive x direction. The initial state is the up-polarized state for Figs. 2(a) and 2(b) and the down-polarized state for Figs. 2(c) and 2(d). The anisotropy constant during the pulse is assumed to be $K_p = 1.4$ mJ/m^2. The DMI constant during the pulse is assumed to be $D_p = 0.5$ mJ/m ($D_p = -0.5$ mJ/m) for the positive (negative) voltage pulse.

In all panels, m_z is almost zero at the end of the pulse ($t = 1$ ns), which means that the almost in-plane polarized magnetic state is realized. After turning off the voltage, m_z increases or decreases with an increase of t depending on the sign of the voltage. For the up-polarized initial state ($m_z = 1$), the magnetization is not switched by the positive voltage pulse but is switched to the down-polarized state ($m_z = -1$) by the negative voltage pulse, as shown in Figs. 2(a) and 2(b). For the down-polarized initial state ($m_z = -1$), the magnetization is not switched by the negative voltage pulse but is switched to the up-polarized state ($m_z = 1$) by the positive voltage pulse, as shown in Figs. 2(c) and 2(d). These results clearly show that the magnetization direction of the final state is determined by the polarity of the voltage pulse irrespective of the initial state.

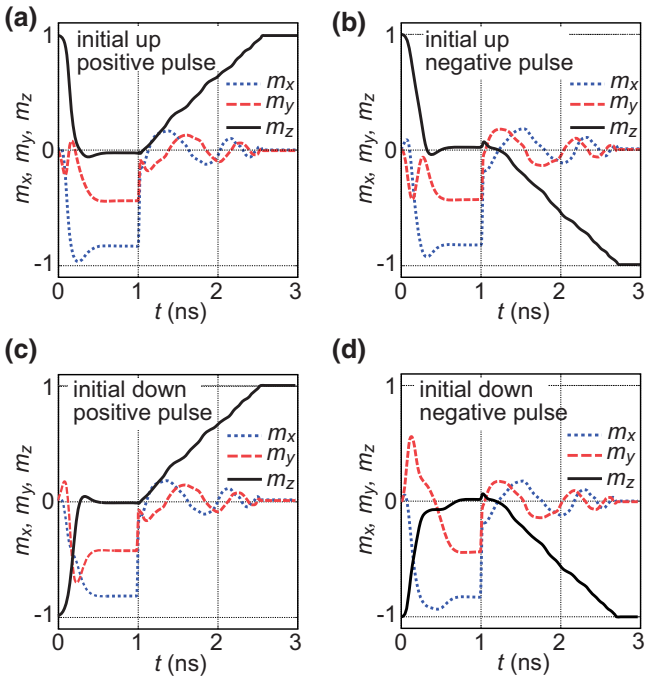

FIG. 2. Time evolution of the x, y, and z components of the space-averaged magnetization unit vector, m_x, m_y, and m_z. (a) The results for the up-polarized initial state with positive voltage pulse ($K_p = 1.4$ mJ/m^2, $D_p = 0.5$ mJ/m). The blue dotted, red dashed, and black solid curves represent m_x, m_y, and m_z, respectively. (b) The same plot for the up-polarized initial state with negative voltage pulse ($K_p = 1.4$ mJ/m^2, $D_p = -0.5$ mJ/m). (c) The same plot for the down-polarized initial state with positive voltage pulse ($K_p = 1.4$ mJ/m^2, $D_p = 0.5$ mJ/m). (d) The same plot for the down-polarized initial state with negative voltage pulse ($K_p = 1.4$ mJ/m^2, $D_p = -0.5$ mJ/m).

Figures 3(a) and 3(b) show the snapshots of the magnetization vectors at $t = 0, 1, 2, 3$ ns for the up-polarized initial state. The sign of the voltage pulse is positive for Fig. 3(a) and negative for Fig. 3(b). The red shading represents the positive m_z, while the blue shading represents the negative m_z. The magnetization configuration at the end of the pulse ($t = 1$ ns) is quite different between the positive and negative voltage pulses. For the positive voltage pulse, m_z at the bottom left corner is positive and that at the top right corner is negative, as shown in the second panel of Fig. 3(a). For the negative voltage pulse, m_z at the bottom left corner is negative and m_z at the top right corner is positive, as shown in the second panel of Fig. 3(b).

For the positive voltage pulse, the up-polarized initial state does not switch to the down-polarized state but

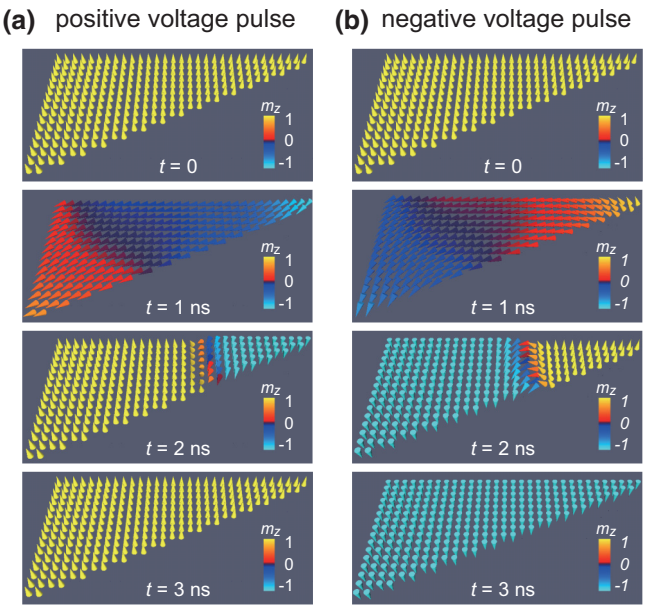

FIG. 3. Snapshots of the magnetization vectors for the up-polarized initial state. (a) The snapshots for the positive voltage pulse. From top to bottom $t = 0$, 1, 2, 3 ns. The red shading represents the positive m_z, while the blue shading represents the negative m_z. (b) The same plot for the negative voltage pulse.

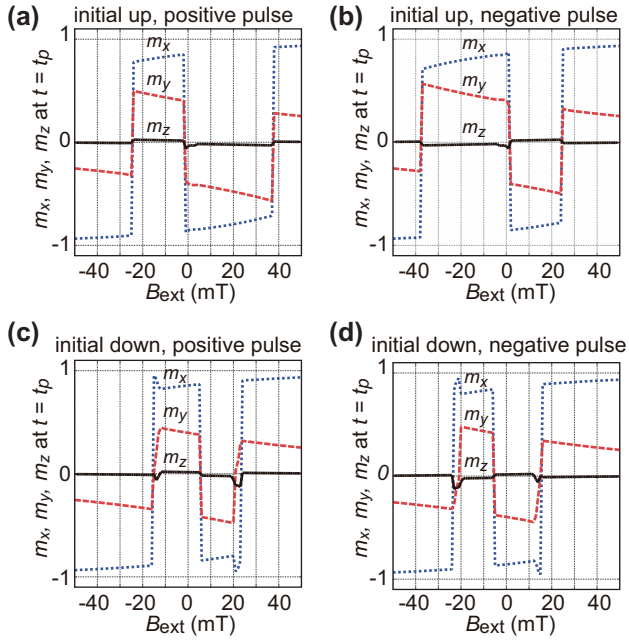

FIG. 4. The x, y, and z components of the space-averaged magnetization unit vector, m_x, m_y, and m_z at the end of the pulse. (a) The results for the up-polarized initial state with positive voltage pulse ($K_p = 1.4$ mJ/m^2, $D_p = 0.5$ mJ/m). The blue dotted, red dashed, and black solid curves represent m_x, m_y, and m_z, respectively. (b) The same plot for the up-polarized initial state with negative voltage pulse ($K_p = 1.4$ mJ/m^2, $D_p = -0.5$ mJ/m). (c) The same plot for the down-polarized initial state with positive voltage pulse ($K_p = 1.4$ mJ/m^2, $D_p = 0.5$ mJ/m). (d) The same plot for the down-polarized initial state with negative voltage pulse ($K_p = 1.4$ mJ/m^2, $D_p = -0.5$ mJ/m).

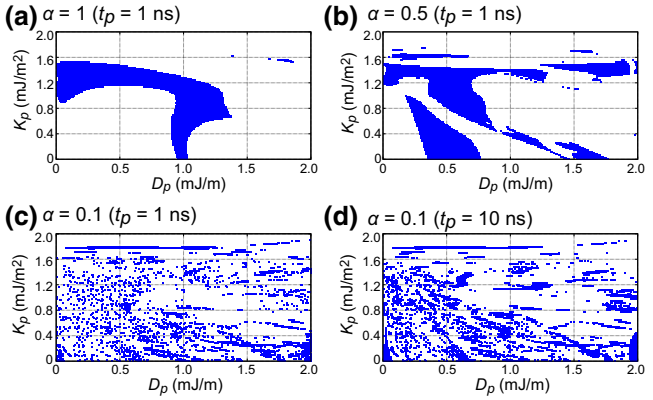

FIG. 5. Switching diagram in terms of D_p and K_p. The external magnetic field is $B_{ext} = 10$ mT. (a) The results for $\alpha = 1$ and $t_p = 1$ ns. The regions where the deterministic switching is available are represented by the shaded areas. (b) The same plot for $\alpha = 0.5$ and $t_p = 1$ ns. (c) The same plot for $\alpha = 0.1$ and $t_p = 1$ ns. (d) The same plot for $\alpha = 0.1$ and $t_p = 10$ ns.

returns to the up-polarized state. Once the voltage is turned off, the magnetic moments around the bottom left corner tilt upward to form an up-polarized domain and those around the top right corner tilt downwards to form a down-polarized domain, as shown in the third panel of Fig. 3(a). Between the up-polarized and down-polarized domains, there appears a narrow domain wall that moves to the top right corner to reduce the domain wall energy. Finally, the domain wall is swept out from the magnet and the up-polarized state is recovered within 3 ns.

Application of the negative voltage pulse switches the magnetization from the up-polarized state to the down-polarized state as shown in Fig. 3(b). After turning off the voltage pulse, the magnetic moments around the bottom left corner tilt downward to form a down-polarized domain and those around the top right corner tilt upward to form an up-polarized domain, as shown in the third panel of Fig. 3(b). The domain wall between these two domains moves to the top right corner and the magnetic state is switched to the down-polarized state within 3 ns.

As shown in the second panels of Figs. 3(a) and 3(b), the most magnetization vectors at the end of the pulse point to the negative x direction even though a B_{ext} of 10 mT is applied in the positive x direction, which implies that 10 mT is not large enough to align the magnetization vectors along B_{ext}. Figures 4(a)–4(d) show the B_{ext} dependence of m_x, m_y, and m_z at the end of the pulse. The parameters other than B_{ext} are the same as those in Figs. 2 and 3. The magnetization configuration and, therefore, the values of m_x, m_y, and m_z suddenly change at certain values of B_{ext}. At large B_{ex} ($|B_{ex}| \geq 40$ mT), m_x has the same sign as B_{ext}, i.e., the most magnetization vectors are aligned long the external magnetic field. Comparing Fig. 4(a) with Fig. 4(b), or 4(c) with 4(d), we note that the magnetization configuration at the end of the pulse has the symmetry with respect to the following transformation: $\{B_{ext}, D_p, m_x, m_y\} \rightarrow \{-B_{ext}, -D_p, -m_x, -m_y\}$. Assuming that the magnetic moments are placed on a two-dimensional plane, one can easily show that the LLG equation has the same symmetry.

Let us discuss the parameter range where deterministic switching is available. Figure 5(a) summarizes the simulation results for various values of D_p and K_p with $\alpha = 1$. The simulations are performed in the range of $0.01 \leq D_p \leq 2$ mJ/m and $0 \leq K_p \leq 2$ mJ/m^2. The pulse width is $t_p = 1$ ns and the external magnetic field of $B_{ext} = 10$ mT is applied in the positive x direction. The parameters (D_p, K_p), where the deterministic switching is available, are plotted by the blue rectangles, most of which bunch around the lines with $K_p \simeq 1.4$ mJ/m^2 and $D_p \simeq 1$ mJ/m. The deterministic switching fails for large K ($\gtrsim 1.6$ mJ/m^2) because the magnetic moments remain almost perpendicular to the plane at the end of the pulse. At around $K_p \simeq 1.4$ mJ/m^2, the uniaxial anisotropy field is almost canceled by the demagnetization field. Therefore, most magnetic moments are aligned in the plane and the

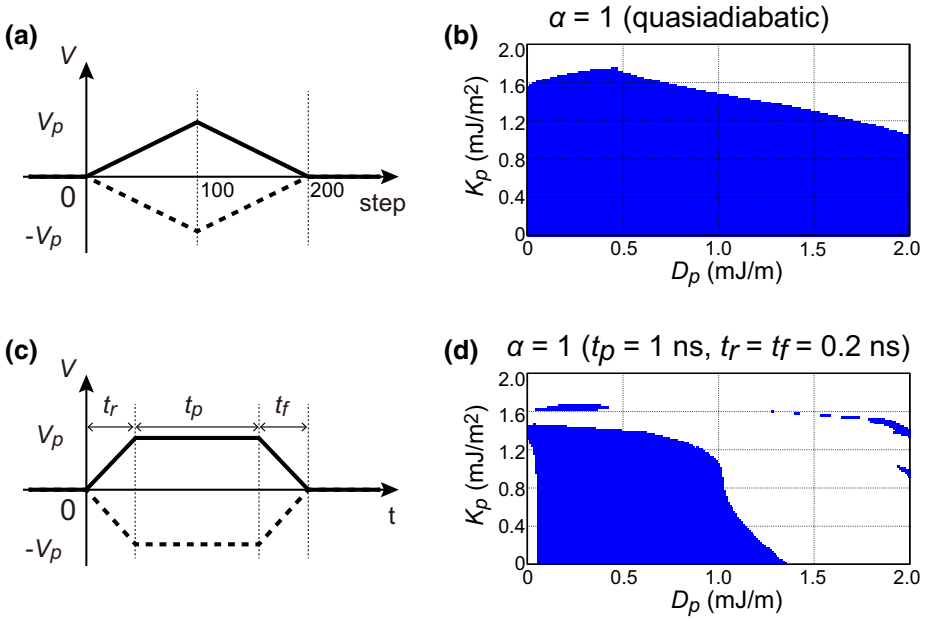

FIG. 6. (a) The quasiadiabatic evolution of the positive (solid) and negative (dotted) voltage is plotted as a function of the step. The absolute value of the voltage is discretized with 100 points, i.e., we take 100 steps to turn on the voltage and another 100 steps to turn off the voltage. At each voltage, the micromagnetic simulation is performed until the magnetic moments are relaxed. (b) The quasiadiabatic switching diagram for $\alpha = 1$. (c) Time (t) dependence of the voltage V for the positive (solid) and negative (dotted) voltage pulse with amplitude of V_p, where t_p, t_r, and t_f denote the rise time, the duration, and the fall time of the pulse, respectively. (d) The pulse switching diagram for $\alpha = 1$, $t_p = 1$ ns, $t_r = t_f = 0.2$ ns.

nucleation core at the corners can easily be created by the small value of D_p. For small K ($\lesssim 1.2$ mJ/m^2), the switching region is limited at around $D_p \simeq 1$ mJ/m. As shown later, this switching region can be spread down to the lower values of D_p by introducing the rise and fall time to the square wave pulse.

Figures 5(b) and 5(c) are the same plot for $\alpha = 0.5$ and 0.1, respectively. For $\alpha = 0.5$, the switching region splits into several small pieces and is scattered, as shown in Fig. 5(b). Also, there appear some switching regions at large K_p ($\gtrsim 1.6$ mJ/m^2). A further decrease of α down to 0.1 scatters the switching region into very fine pieces, as shown in Fig. 5(c). In Fig. 5(d), we plot the results for $\alpha = 0.1$ and $t_p = 10$ ns, which is long enough for magnetization to relax. Comparing Fig. 5(d) with Fig. 5(c), some switching regions are clustered, but the difference between them is not significant. These results imply that the precessional motion of magnetic moments plays an important role in switching failure, i.e., the magnetic moments do not relax into the equilibrium state but into one of the quasiequilibrium states.

In order to clarify the effect of the precessional motion on switching, we calculate the quasiadiabatic dynamics of magnetic moments. As shown in Fig. 6(a), the absolute value of the voltage pulse V_p is discretized with 100 points, i.e., we take 100 steps to turn on the voltage and another 100 steps to turn off the voltage. At each voltage, the micromagnetic simulation is performed until the magnetic moments are relaxed. Figure 6(b) is the switching diagram based on the quasiadiabatic simulations with $\alpha = 1$. Comparing Fig. 6(b) with Fig. 5(a), one can clearly see that the failure of switching for $K_p \lesssim 1.2$ mJ/m^2 is due to the precessional motion.

Because we assume the square shape for the voltage pulse, the effective field suddenly changes, and the large precessional torque is exerted on the magnetic moments, at the beginning and end of the pulse. The results shown in Figs. 6(a) and 6(b) suggest that the introduction of the rise and fall time to the pulse will spread the switching region in Fig. 5(a).

We performe the simulations under the voltage pulse with the rise and fall time shown in Fig. 6(c). The duration of the pulse is assumed to be $t_p = 1$ ns and the rise time and the fall time are assumed to be $t_r = t_f = 0.2$ ns. The other parameters are the same as in Fig. 5(a). The switching diagram is shown in Fig. 6(d). Introduction of the rise and fall time of 0.2 ns spreads the switching region, i.e., most of the unswitching region in the bottom left part of Fig. 5(a) becomes the switching region in Fig. 6(d).

TABLE I. $B_{\rm ext}$ and D_p dependence of the switching results for $\alpha = 1$, $K_p = 1.4$ mJ/m^2, $t_r = t_f = 0.2$ ns, and $t_p = 1$ ns. The value of $B_{\rm ext}$ is shown in units of mT. The value of D_p is shown in units of mJ/m. A check mark indicates that the deterministic switching succeeds. A cross indicates that the deterministic switching fails.

$D_p \backslash B_{\rm ext}$	0	1	2	3	4	5	6	7	8	9	10
0.01	×	×	×	✓	✓	✓	✓	✓	✓	✓	✓
0.02	×	×	×	✓	✓	✓	✓	✓	✓	✓	✓
0.05	×	×	✓	✓	✓	✓	✓	✓	✓	✓	✓
0.1	×	×	✓	✓	✓	✓	✓	✓	✓	✓	✓
0.2	×	×	×	✓	✓	✓	✓	✓	✓	✓	✓
0.5	×	×	×	×	×	✓	✓	✓	✓	✓	×

Table I summarizes the results for various values of $B_{\rm ext}$ and D_p. The anisotropy constant during the pulse is assumed to be $K_p = 1.4$ mJ/m^2. The other parameters are the same as in Fig. 6(d). Note that the deterministic switching fails for small values of $B_{\rm ext}$. At $B_{\rm ext} = 0$, the LLG equation is invariant under the transformation of $\{D_p, m_x, m_y\} \rightarrow \{-D_p, -m_x, -m_y\}$. Because of this symmetry, the dynamics of the z component of the magnetic moments and, therefore, the magnetic state after the voltage pulse are the same for both the positive and the negative voltage pulses. Application of the external field is necessary to break the symmetry of the LLG equation and make the dynamics of m_z different between the positive and the negative voltage pulses.

V. SUMMARY

In summary, based on the micromagnetic simulations, it is demonstrated that the voltage-induced changes of MA and DMI can switch the magnetization of a right-triangle magnet under an in-plane magnetic field. The magnetic state after application of the voltage pulse is determined by the polarity of the voltage irrespective of the initial magnetic state. The mechanism of switching and the conditions for the shape of the magnetic element and material parameters are clarified. The proposed deterministic switching provides a fast and low-power writing method for VCMRAMs without preread.

ACKNOWLEDGMENTS

This work was partially supported by the ImPACT Program of the Council for Science, Technology and Innovation (Cabinet Office, Government of Japan).

[1] M. Weisheit, S. Fahler, A. Marty, Y. Souche, C. Poinsignon, and D. Givord, Electric field-induced modification of magnetism in thin-film ferromagnets, Science **315**, 349 (2007).

[2] T. Maruyama, Y. Shiota, T. Nozaki, K. Ohta, N. Toda, M. Mizuguchi, A. A. Tulapurkar, T. Shinjo, M. Shiraishi, S. Mizukami, Y. Ando, and Y. Suzuki, Large voltage-induced magnetic anisotropy change in a few atomic layers of iron, Nat. Nanotechnol. **4**, 158 (2009).

[3] T. Nozaki, Y. Shiota, M. Shiraishi, T. Shinjo, and Y. Suzuki, Voltage-induced perpendicular magnetic anisotropy change in magnetic tunnel junctions, Appl. Phys. Lett. **96**, 3 (2010).

[4] Yoichi Shiota, Takayuki Nozaki, Frédéric Bonell, Shinichi Murakami, Teruya Shinjo, and Yoshishige Suzuki, Induction of coherent magnetization switching in a few atomic layers of FeCo using voltage pulses, Nat. Mater. **11**, 39 (2011).

[5] Takayuki Nozaki, Hiroko Arai, Kay Yakushiji, Shingo Tamaru, Hitoshi Kubota, Hiroshi Imamura, Akio Fukushima, and Shinji Yuasa, Magnetization switching assisted by high-frequency-voltage-induced ferromagnetic resonance, Appl. Phys. Express **7**, 093005 (2014).

[6] Wen Chin Lin, Po Chun Chang, Cheng Jui Tsai, Tsung Chun Shieh, and Fang Yuh Lo, Voltage-induced reversible changes in the magnetic coercivity of Fe/ZnO heterostructures, Appl. Phys. Lett. **104**, 1 (2014).

[7] Pedram Khalili Amiri, Juan G. Alzate, Xue Qing Cai, Farbod Ebrahimi, Qi Hu, Kin Wong, Cécile Grèzes, Hochul Lee, Guoqiang Yu, Xiang Li, Mustafa Akyol, Qiming Shao, Jordan A. Katine, Jürgen Langer, Berthold Ocker, and Kang L. Wang, Electric-field-controlled magnetoelectric RAM: Progress, challenges, and scaling, IEEE Trans. Magn. **51**, 1 (2015).

[8] S. Kanai, F. Matsukura, and H. Ohno, Electric-field-induced magnetization switching in CoFeB/MgO magnetic tunnel junctions with high junction resistance, Appl. Phys. Lett. **108**, 2014 (2016).

[9] C. Grezes, F. Ebrahimi, J. G. Alzate, X. Cai, J. A. Katine, J. Langer, B. Ocker, P. Khalili Amiri, and K. L. Wang, Ultra-low switching energy and scaling in electric-field-controlled nanoscale magnetic tunnel junctions with high resistance-area product, Appl. Phys. Lett. **108**, 3 (2016).

[10] Kamaram Munira, Sumeet C. Pandey, Witold Kula, and Gurtej S. Sandhu, Voltage-controlled magnetization switching in MRAMs in conjunction with spin-transfer torque and applied magnetic field, J. Appl. Phys. **120**, 203902 (2016).

[11] Takayuki Nozaki, Anna Kozio-Rachwa, Witold Skowroński, Vadym Zayets, Yoichi Shiota, Shingo Tamaru, Hitoshi Kubota, Akio Fukushima, Shinji Yuasa, and Yoshishige Suzuki, Large Voltage-Induced Changes in the Perpendicular Magnetic Anisotropy of an MgO-Based Tunnel Junction with an Ultrathin Fe Layer, Phys. Rev. Appl. **5**, 044006 (2016).

[12] Yoichi Shiota, Takayuki Nozaki, Shingo Tamaru, Kay Yakushiji, Hitoshi Kubota, Akio Fukushima, Shinji Yuasa, and Yoshishige Suzuki, Evaluation of write error rate for voltage-driven dynamic magnetization switching in magnetic tunnel junctions with perpendicular magnetization, Appl. Phys. Express **9**, 013001 (2016).

[13] Takayuki Nozaki, Anna Kozio-Rachwa, Masahito Tsujikawa, Yoichi Shiota, Xiandong Xu, Tadakatsu Ohkubo, Takuya Tsukahara, Shinji Miwa, Motohiro Suzuki, Shingo Tamaru, Hitoshi Kubota, Akio Fukushima, Kazuhiro Hono, Masafumi Shirai, Yoshishige Suzuki, and Shinji Yuasa, Highly efficient voltage control of spin and enhanced interfacial perpendicular magnetic anisotropy in iridium-doped Fe/MgO magnetic tunnel junctions, NPG Asia Mater. **9**, e451 (2017).

[14] Ie E. Dzyaloshinskii, On the magneto-electrical effect in antiferromagnets, J. Soviet Phys. JETP **10**, 628 (1960).

[15] Tôru Moriya, Anisotropic superexchange interaction and weak ferromagnetism, Phys. Rev. **120**, 91 (1960).

[16] A. Crépieux and C. Lacroix, Dzyaloshinsky-Moriya interactions induced by symmetry breaking at a surface, J. Magn. Magn. Mater. **182**, 341 (1998).

[17] M. Bode, M. Heide, K. von Bergmann, P. Ferriani, S. Heinze, G. Bihlmayer, A. Kubetzka, O. Pietzsch, S. Blügel, and R. Wiesendanger, Chiral magnetic order at surfaces driven by inversion asymmetry, Nature **447**, 190 (2007).

[18] P. Ferriani, K. von Bergmann, E. Y. Vedmedenko, S. Heinze, M. Bode, M. Heide, G. Bihlmayer, S. Blügel, and R. Wiesendanger, Atomic-Scale Spin Spiral with a Unique

Rotational Sense: Mn Monolayer on W(001), Phys. Rev. Lett. **101**, 027201 (2008).

[19] S. Muhlbauer, B. Binz, F. Jonietz, C Pfleiderer, A Rosch, A Neubauer, Robert Georgii, and P. Boni, Skyrmion lattice in a chiral magnet, Science **323**, 915 (2009).

[20] A. Neubauer, C. Pfleiderer, B. Binz, A. Rosch, R. Ritz, P. G. Niklowitz, and P. B"oni, Topological Hall Effect in the A Phase of MnSi, Phys. Rev. Lett. **102**, 186602 (2009).

[21] C. Pappas, E. Lelièvre-Berna, P. Falus, P. M. Bentley, E. Moskvin, S. Grigoriev, P. Fouquet, and B. Farago, Chiral Paramagnetic Skyrmion-like Phase in MnSi, Phys. Rev. Lett. **102**, 197202 (2009).

[22] André Thiaville, Stanislas Rohart, Émilie Jué, Vincent Cros, and Albert Fert, Dynamics of Dzyaloshinskii domain walls in ultrathin magnetic films, EPL **100**, 57002 (2012).

[23] Albert Fert, Vincent Cros, and João Sampaio, Skyrmions on the track, Nat. Nanotechnol. **8**, 152 (2013).

[24] Kwang-Su Ryu, Luc Thomas, See-Hun Yang, and Stuart Parkin, Chiral spin torque at magnetic domain walls, Nat. Nanotechnol. **8**, 527 (2013).

[25] Satoru Emori, Uwe Bauer, Sung Min Ahn, Eduardo Martinez, and Geoffrey S. D. Beach, Current-driven dynamics of chiral ferromagnetic domain walls, Nat. Mater. **12**, 611 (2013).

[26] Jacob Torrejon, Junyeon Kim, Jaivardhan Sinha, Seiji Mitani, Masamitsu Hayashi, Michihiko Yamanouchi, and Hideo Ohno, Interface control of the magnetic chirality in CoFeB/MgO heterostructures with heavy-metal underlayers, Nat. Commun. **5**, 1 (2014).

[27] Kohei Nawaoka, Shinji Miwa, Yoichi Shiota, Norikazu Mizuochi, and Yoshishige Suzuki, Voltage induction of interfacial Dzyaloshinskii-Moriya interaction in Au/Fe/MgO artificial multilayer, Appl. Phys. Express **8**, 063004 (2015).

[28] Dong Soo Han, Nam Hui Kim, June Seo Kim, Yuxiang Yin, Jung Woo Koo, Jaehun Cho, Sukmock Lee, Mathias Kläui, Henk J. M. Swagten, Bert Koopmans, and Chun Yeol You, Asymmetric hysteresis for probing Dzyaloshinskii-Moriya interaction, Nano Lett. **16**, 4438 (2016).

[29] T. H. R. Skyrme, A unified field theory of mesons and baryons, Nucl. Phys. **31**, 556 (1962).

[30] S. Kanai, Y. Nakatani, M. Yamanouchi, S. Ikeda, H. Sato, F. Matsukura, and H. Ohno, Magnetization switching in a CoFeB/MgO magnetic tunnel junction by combining spin-transfer torque and electric field-effect, Appl. Phys. Lett. **104**, 9 (2014).

[31] Arne Vansteenkiste, Jonathan Leliaert, Mykola Dvornik, Mathias Helsen, Felipe Garcia-Sanchez, and Bartel Van Waeyenberge, The design and verification of MuMax3, AIP Adv. **4**, 107133 (2014).